

Microlensing optical depth as a function of source apparent magnitude

Alexander Wood ^{*}

Jodrell Bank Observatory, University of Manchester, Macclesfield, Cheshire SK11 9DL

Accepted Received; in original form

ABSTRACT

Measurements of the microlensing optical depth τ towards the Galactic bulge appear to depend on the method used to obtain them. Those values based on the lensing of red clump giants (RCGs) appear to be significantly lower than those based on the lensing of all stars along the line of sight. This discrepancy is still not understood. Through Monte Carlo simulations, it is found that the discrepancy cannot be explained by a dependance on the flux limits of the two methods. The optical depth is expected to be generally constant as a function of source apparent magnitude for $I_0 \gtrsim 13.0$, except in the range $13.5 \lesssim I_0 \lesssim 15.5$. Here many RCGs are detected, causing a significant oscillation in τ . The amplitude of this oscillation is a function of the inclination angle of the Galactic bar, θ_{bar} , which may thus be constrained. A further constraint comes from a similar dependance of τ with θ_{bar} : combining the predicted trends with the measured values provides 1σ upper limits, which exclude the large bar angles recently reported by the GLIMPSE and EROS surveys. The latest survey data from EROS-2 appear to show the predicted τ oscillation, though currently at a low significance. However, a further sign comes from EROS-2 event counts, which show a clear skew towards fainter magnitudes.

Key words: gravitational lensing – galaxies: bulges – galaxies: structure

1 INTRODUCTION

Thousands of microlensing events in our Galaxy have so far been discovered by OGLE (e.g. Woźniak et al. 2001), MACHO (e.g. Thomas et al. 2005), MOA (e.g. Sumi et al. 2003) and EROS (e.g. Afonso et al. 2003), with many more detected

every year¹. One of the most important measurements that can be made from these observations is of the optical depth, τ – the probability of seeing a microlensing event. However, the measured value appears to depend strongly on the method used to obtain it.

^{*} Email: A.A.Wood@postgrad.manchester.ac.uk

¹ Real-time alerts are available online, e.g. the OGLE Early Warning System: www.astrouw.edu.pl/~ogle/ogle3/ews/ews.html

2 Wood

Popowski et al. (2005) reported $\tau_{\text{MACHO}} = 2.17_{-0.38}^{+0.47} \times 10^{-6}$ at $(l, b) = (1.50^\circ, -2.68^\circ)$, and more recently from the OGLE-II survey, Sumi et al. (2006) found $\tau_{\text{OGLE}} = 2.55_{-0.46}^{+0.57} \times 10^{-6}$ at $(l, b) = (1.16^\circ, -2.75^\circ)$. The MACHO value was based on the lensing of 42 red clump giants (RCGs), and used standard photometric fitting. The OGLE analysis instead used difference image analysis (DIA), but was similarly based on the lensing of 32 red giants, red super giants and RCGs, and obtained an optical depth consistent with the previous MACHO result. However, both these values are significantly lower than two other recent measurements, which were based on the lensing of all stars. Using 28 DIA events, Sumi et al. (2003) found $\tau_{\text{MOA}} = 3.36_{-0.81}^{+1.11} \times 10^{-6} [0.77/(1 - f_{\text{disc}})]$, where f_{disc} is the contribution from disc sources – the coordinates of this value are given in Sumi et al. (2006): $(l, b) = (3.0^\circ, -3.8^\circ)$. Alcock et al. (2000) had previously found $\tau = 3.23_{-0.50}^{+0.52} \times 10^{-6} [0.75/(1 - f_{\text{disc}})]$ at $(l, b) = (2.68^\circ, -3.35^\circ)$, from 99 MACHO DIA events. The latest measurement comes from the EROS-2 survey of bulge RCGs, which yielded 120 events: Hamadache et al. (2006) give the trend $\tau_{\text{EROS}} = (1.62 \pm 0.23) \exp[-a(|b| - 3 \text{ deg})] \times 10^{-6}$, where $a = (0.43 \pm 0.16 \text{ deg}^{-1})$, in the latitude range $1.4^\circ < |b| < 7.0^\circ$. This agrees well with previous EROS values, and with the recent MACHO and OGLE-II measurements.

The question naturally arises as to why the RCG-based optical depths appear to be lower than those from all stars. One possibility is a dependence on the flux limits of the two methods. RCGs are bright; the latter method will include much fainter stars, and so probe sources at greater distances, which will have a higher optical depth (Stanek 1995).

This potential explanation of the discrepancy is investigated using Monte Carlo simulations of Galactic microlensing, and the optical depth as a function of source apparent magnitude is then predicted. The model Galaxy is barred, and in light of observations by the *Spitzer Space Telescope* (SST), that support a bar inclination angle much larger than suggested by previous studies (see §2.1), the effect on the expected τ of changing the bar angle is determined. Combining these results with the observed optical depths, upper limits are placed on the bar angle. §2 describes the model. The results and discussion are presented in §3: the model results are given in §3.1,

and comparisons are made with the latest EROS-2 data in §3.2. A summary and conclusions follow in §4.

2 THE MODEL

2.1 Bulge and disc mass models

The mass models and parameters of the Galactic bulge (bar) and disc are as described in Wood & Mao (2005). They are based on those of Han & Gould (2003), who empirically normalised the G2 bulge model of Dwek et al. (1995, table 1) with *Hubble Space Telescope* star counts, and extended the local disc model of Zheng et al. (2001) to the whole disc. Dwek et al. tested a series of models against images of the Galactic bulge from the *Cosmic Background Explorer* (COBE) satellite, and found their G2 model to provide one of the best fits. This model bar extends from 3–13 kpc and is inclined to the Galactic centre line of sight (LOS) at an angle of $\theta_{\text{bar}} = 13.4^\circ$. Gerhard (2002) states that physical models can be found for the COBE bar with angles in the range $15^\circ \lesssim \theta_{\text{bar}} \lesssim 35^\circ$, and many studies assume $\theta_{\text{bar}} \approx 20^\circ$. However, more recent data from GLIMPSE (Galactic Legacy Infrared Mid-Plane Survey Extraordinaire), using the SST, support a much larger value of $(44 \pm 10)^\circ$ (Benjamin et al. 2005), while from EROS-2, Hamadache et al. (2006) report $\theta_{\text{bar}} = (49 \pm 8)^\circ$, which is consistent with original OGLE-I results (Stanek et al. 1994). Hence, predictions are also made here for Dwek et al.’s E2 model, which has the largest bar angle of their models: $\theta_{\text{bar}} = 41.3^\circ$.

2.2 Source population

The expected τ_{OGLE} , τ_{MACHO} and τ_{MOA} are to be calculated. Therefore for each LOS, the apparent magnitude distribution of the model sources must match the observed distribution. Sumi (2004) fitted the *I*-band stellar distributions in 48 OGLE-II Galactic bulge fields with the power-law plus Gaussian luminosity function

$$\phi_I(I) = p_0 10^{p_1 I} + p_2 \exp \left[-\frac{(I - \langle I \rangle_{\text{RC}})^2}{2\sigma_{I,\text{RC}}^2} \right], \quad (1)$$

where p_0 , p_1 , p_2 and $\sigma_{I,\text{RC}}$ are free parameters, and $\langle I \rangle_{\text{RC}}$ is measured as described in his paper. The power-law part contains red giants and bright main-sequence stars, which

	l ($^{\circ}$)	b ($^{\circ}$)	Angular separation ($^{\circ}$)
OGLE	1.16	-2.75	0.40
Field 34	1.35	-2.40	
MACHO	1.50	-2.68	0.28
Field 20	1.68	-2.47	
MOA	3.0	-3.8	0.6
Field 36	3.16	-3.20	

Table 1. Selection of the OGLE-II Galactic bulge fields that are closest to the lines of sight of the OGLE, MACHO (RCG) and MOA optical depth measurements.

lie throughout the bar. The Gaussian component consists of RCGs, which in the model here are more concentrated in the central part of the bulge, occupying the region 6–10 kpc. (This concentration is found to improve the match to the observed magnitude distributions, and is not unreasonable, as RCGs are older, evolved stars, and hence more likely to exist only in more densely populated regions).

Sumi (2004) thus provides, for each of these fields, an observed distribution of apparent magnitude. The positions of these fields are listed in table 1 of Udalski et al. (2002).

The fields closest to the OGLE, MACHO (RCG) and MOA lines of sight are selected, as shown in Table 1. The MACHO (DIA) LOS is not considered, as explained below.

As described in §2.3, the apparent magnitude of each source is calculated by first assigning it an absolute magnitude, and then correcting for its distance. Hence for each LOS a separate model distribution of absolute magnitude is required that will, with distance corrections, reproduce the observed distribution of apparent magnitude. Of course in reality the absolute magnitude distribution should be virtually the same for each direction in Table 1, since over these small angular separations the mass function is expected to vary little. Here, the artificial absolute magnitude distributions are only used as a means to ensure the model distributions of apparent magnitude match those observed for each direction. It is assumed that the forms of the two distributions are the same, i.e. a power-law plus Gaussian. For each of the three OGLE-II fields listed in Table 1, an appropriate absolute magnitude distribution can easily be generated, by suitably adjusting the (extinction-corrected) fitted parameters of the apparent magnitude distribution found by Sumi (2004). (These parameters

	$I_{0,\min}$	$I_{0,\max}$
OGLE	12.1	15.3
MACHO	13.9	16.2
	($V = 16.37$)	($V = 20.19$)
MOA	13.6	20.8

Table 2. Defined ranges of detectable, extinction-corrected apparent magnitudes for OGLE, MACHO and MOA.

are not given in Sumi (2004), and are provided by T. Sumi, private communication).

Sumi et al. (2003, table 5) and Sumi et al. (2006, table 4) list the extinction-corrected I -band apparent magnitudes of all the MOA and OGLE sources used in their respective measurements of τ . The minimum and maximum magnitudes given in each case are taken to define ranges of detectable apparent magnitudes. Popowski et al. (2005), in their table 2, provide uncorrected V -band apparent magnitudes. Since these MACHO sources are all RCGs, their apparent magnitudes are converted to I -band using the following relation for RCGs from Sumi et al. (2003):

$$I = (1.45 \pm 0.12) (V - I) + 12.7. \quad (2)$$

MACHO source extinction is then accounted for by simply shifting the minimum and maximum MACHO magnitudes by the mean A_I for the corresponding OGLE-II field, as given in table 3 of Sumi (2004): for field 20, $A_I = 0.951$. (Strictly speaking the extinction should instead be calculated for each source individually, but this is neglected as in the region occupied by the model RCGs, A_I varies from the mean value by $\lesssim 0.05$ mag – a negligible amount). Although Alcock et al. (2000) also list the apparent magnitudes of the MACHO sources used in their DIA measurement, these are in V -band and do not consist of only RCGs. Therefore an I -band magnitude range cannot be reliably defined for the model. The defined ranges of detectable, extinction-corrected apparent magnitudes I_0 for OGLE, MACHO and MOA are given in Table 2.

2.3 Optical depth

The expected τ_{OGLE} , for example, can now be calculated as follows. First a distance is chosen for a given source along the OGLE LOS. It is assigned an absolute magnitude using the artificial distribution constructed for the nearest OGLE-II

	$(l, b) (^{\circ})$	τ_{obs} ($\times 10^{-6}$)	$\tau_{\text{model,G2}}$ ($\times 10^{-6}$)	$\tau_{\text{model,E2}}$ ($\times 10^{-6}$)
OGLE	(1.16, -2.75)	$2.55^{+0.57}_{-0.46}$	2.14	1.57
MACHO	(1.50, -2.68)	$2.17^{+0.47}_{-0.38}$	2.19	1.61
MOA	(3.0, -3.8)	$3.36^{+1.11}_{-0.81}$ (2.59 $^{+0.84}_{-0.64}$)	1.38	1.01

Table 3. The expected G2 optical depths agree well with those reported by OGLE and MACHO, but not with MOA’s values. (The numbers in parentheses are without the DIA correction for disc sources – see text).

field, #34. The source’s apparent magnitude is then calculated by accounting for its distance.

If this apparent magnitude falls within the defined range of magnitudes detectable by OGLE, the source is included in the calculation of τ (using equation (5) of Wood & Mao 2005). This process is then repeated for many sources. The expected τ_{MACHO} and τ_{MOA} are similarly calculated.

3 RESULTS AND DISCUSSION

3.1 Model results

Fig. 1 shows that the model well reproduces the observed distributions of apparent magnitude for fields 20, 34 and 36. Table 3 shows that the expected values of τ_{OGLE} and τ_{MACHO} also agree well with the observed values, for the G2 model. However, the expected τ_{MOA} lies $\sim 2.4\sigma$ below the reported value. As the MOA measurement is sensitive to *all* sources along the LOS, a correction was applied to account for disc sources. This is expressed by the f_{disc} term in the τ measurements quoted in §1. Such adjustments typically raise τ by ~ 25 per cent. Note that the model underpredicts τ_{MOA} by a much greater margin, hence the disagreement cannot be attributed to the correction applied by MOA. It therefore appears that the discrepancy in the survey measurements cannot be simply explained by a dependance on their different flux limits.

However, there may be other ways in which τ depends on the source flux. So far the predicted optical depths have been calculated by summing over all the source stars whose apparent magnitudes fall within specified ranges. By repeating this process for many small bins of I_0 , τ can be predicted as a function of I_0 . This is plotted in Fig. 2, for the OGLE, MACHO and MOA coordinates ($\tau_{\text{OGLE LOS}}$, $\tau_{\text{MACHO LOS}}$ and $\tau_{\text{MOA LOS}}$, respectively). The detectable magnitude ranges given in Table 2 are also shown. For each LOS the absolute

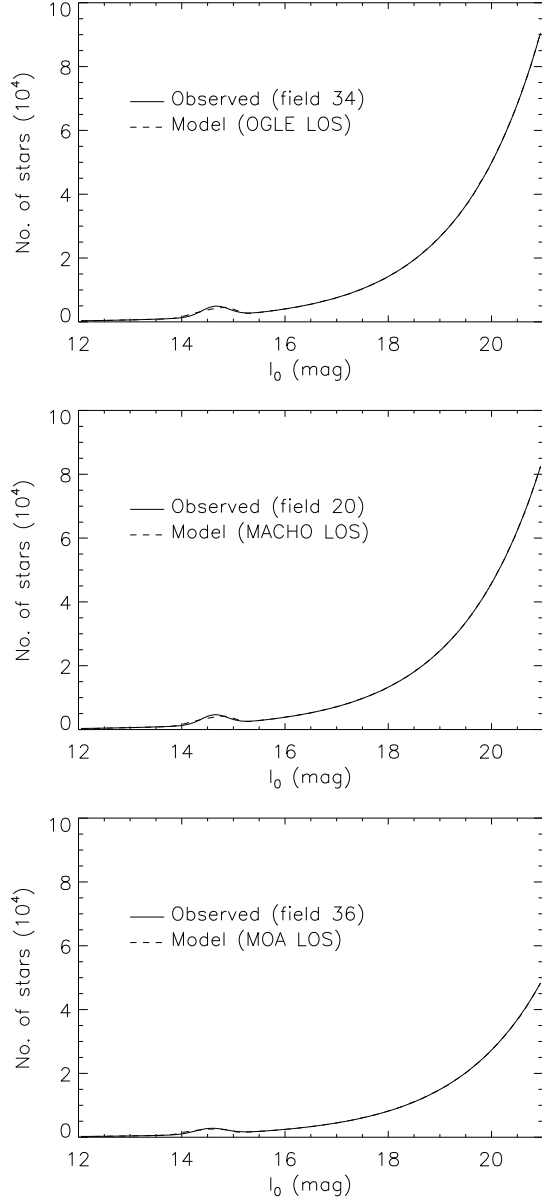


Figure 1. (Top, middle, bottom) panel: apparent magnitude distributions, for stars observed in OGLE-II field (34, 20, 36) by Sumi (2004), and model stars along the (OGLE, MACHO, MOA) LOS. These plots are for the G2 model – there is negligible difference with E2. The model curves are normalised to the same area as the corresponding observed curves.

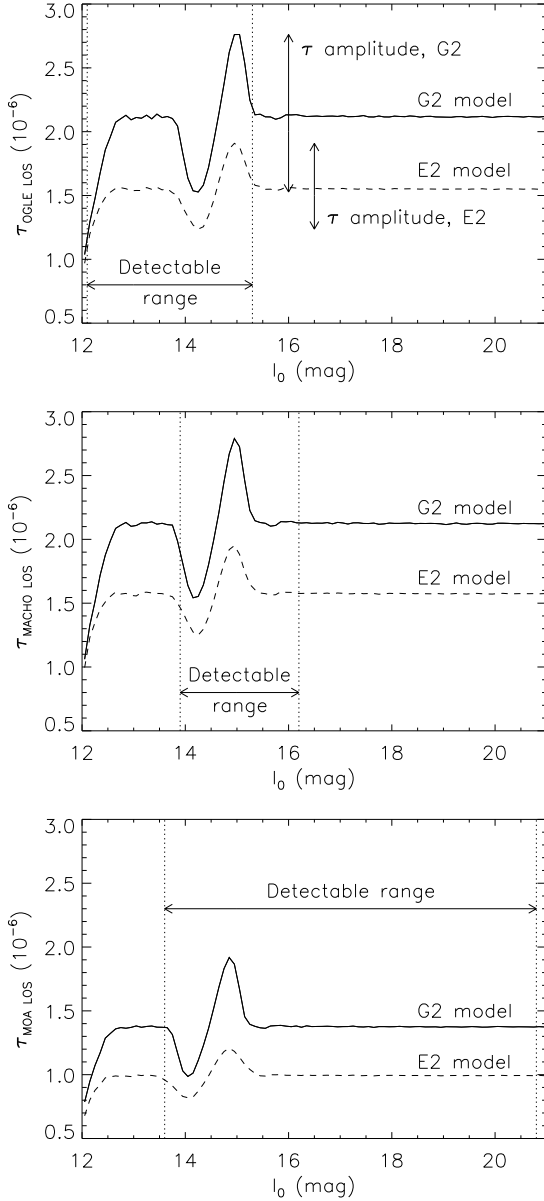


Figure 2. (Top, middle, bottom) panel: expected ($\tau_{\text{OGLE LOS}}$, $\tau_{\text{MACHO LOS}}$, $\tau_{\text{MOA LOS}}$) as a function of source apparent magnitude, for the G2 and E2 models. The detectable magnitude ranges given in Table 2 are shown. In the top panel, the amplitude of the $\tau_{\text{OGLE LOS}}$ oscillation (see text) is indicated for both the G2 and E2 models.

expected value of τ is higher for the G2 bar than the E2, but its trend with magnitude is similar. These trends are explained as follows.

τ increases rapidly over the range $12 \lesssim I_0 \lesssim 13$. Almost all sources of magnitude ~ 12 will be on the near side of the bulge, so as I_0 increases fainter and more distant stars, with higher optical depths, come into view. For $I_0 \gtrsim 15.5$, τ is approximately constant. This is because the power-law part of the source magnitude distribution spans a wide range of I_0 .

Hence these stars can be either bright or faint whether they are near or far, and thus will show little or no correlation between apparent magnitude and distance. So, when calculating the average τ for a given apparent magnitude, the lower optical depth of the closer stars is balanced by the higher τ of those more distant.

In comparison, the Gaussian (RCG) part of the source distribution covers only a very narrow range of absolute magnitudes. The RCGs' distribution in apparent magnitude will be broader, due to variations in their distance, but as they are more concentrated in the centre of the bulge, this broadening is not great. Therefore the vast majority of RCGs will lie within a small range of apparent magnitude, and hence show a strong correlation between apparent magnitude and distance. At $I_0 \approx 14$ we see many RCGs, and they greatly outnumber the other sources. Most of the RCGs at this magnitude lie on the near side of the bulge, and τ is lower. As I_0 increases, the average distance of the RCGs (and so of all sources) being observed shifts towards the far side of the bulge, and τ increases. As I_0 becomes fainter still, $\gtrsim 15$, we see fewer and fewer RCGs, and the average distance of all the observed sources moves back towards the centre of the bulge, where it then remains, and τ becomes approximately constant. The amplitude of this oscillation in τ (hereafter the τ amplitude) caused by the RCGs along the OGLE LOS is indicated in the top panel of Fig. 2.

This strong correlation displayed by the RCGs is illustrated as follows. In Figs. 3 and 4, contours are plotted of source counts as a function of distance and apparent magnitude along each LOS, for the G2 and E2 models, respectively. The two components of the source population are clearly distinguishable. For the G2 model, most of the RCGs appear as a narrow diagonal line in the range $14.0 \lesssim I_0 \lesssim 15.0$. For E2, this region is wider (for a given distance) and shallower. These differences in shape are primarily due to the different bar angles of the G2 and E2 models (13.4° and 41.3° , respectively). The red giants and other stars form a smoother background, with a steep increase in numbers, and a broadening in distance, as I_0 increases. In the top panels of Figs. 3 and 4, the vertical dotted lines indicate slices of this distribution – for the OGLE LOS – that are shown in Figs. 5 and 6, respectively. Finally, the top panel of Fig. 7 gives the average distance of model OGLE

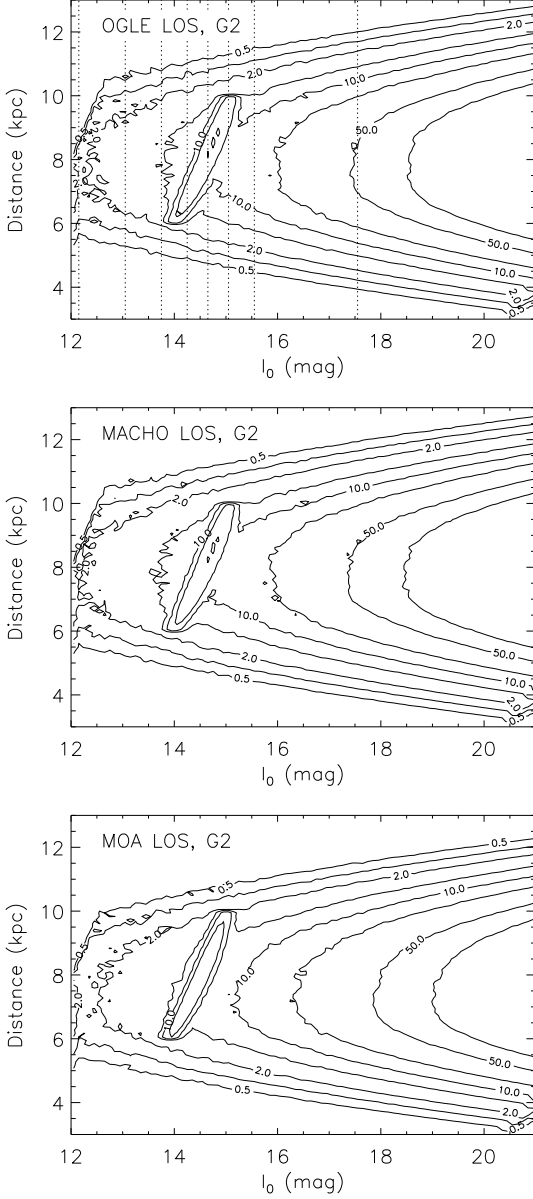


Figure 3. (Top, middle, bottom) panel: G2 model source counts as a function of distance and apparent magnitude, for the (OGLE, MACHO, MOA) coordinates. The RCG component is clearly visible (see text). The vertical dotted lines (top panel) correspond to the slices shown in Fig. 5 (see text). The normalisation is arbitrary. Contour levels are at 0.5, 1.0, 2.0, 5.0, 10.0, 20.0, 50.0 and 100.0.

LOS sources as a function of I_0 . The slice magnitudes are indicated, and the bottom panel shows how they intersect the $\tau_{\text{OGLE LOS}}$ trend from Fig. 2. Note that the trends of average source distance and optical depth with I_0 are almost identical, as would be expected for the reasons given above.

The expected oscillation in τ caused by the RCGs is clearly significant. For example, Fig. 2 shows that the τ amplitude along the OGLE LOS is $\sim 1.2 \times 10^{-6}$. This is a deviation of $\sim \pm 30$ per cent from the approximately constant optical

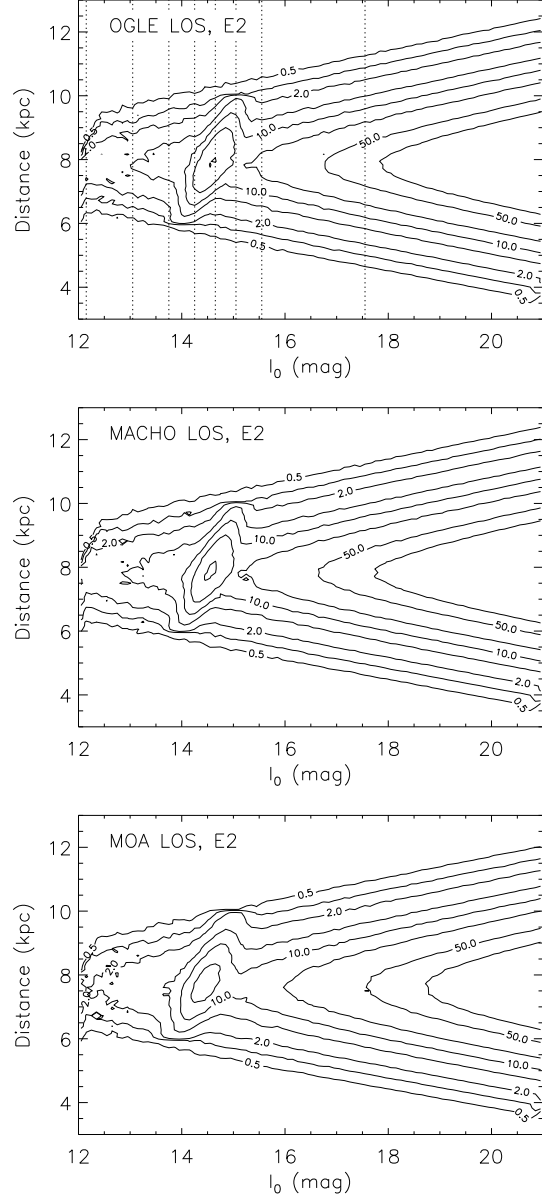


Figure 4. Model source counts as a function of distance and apparent magnitude. Same as Fig. 3, but for the E2 model, with the vertical dotted lines corresponding to the slices shown in Fig. 6 (see text). The normalisation is arbitrary, but consistent with Fig. 3.

depth at fainter magnitudes (hereafter τ_{flat}), where far fewer RCGs are seen: $\tau_{\text{flat}} \approx 2.1 \times 10^{-6}$. For comparison, OGLE's measured value of $2.55^{+0.57}_{-0.46} \times 10^{-6}$ has an uncertainty of only $\sim \pm 20$ per cent, so the predicted oscillation ought to be detectable if enough sources are observed at the correct magnitudes.

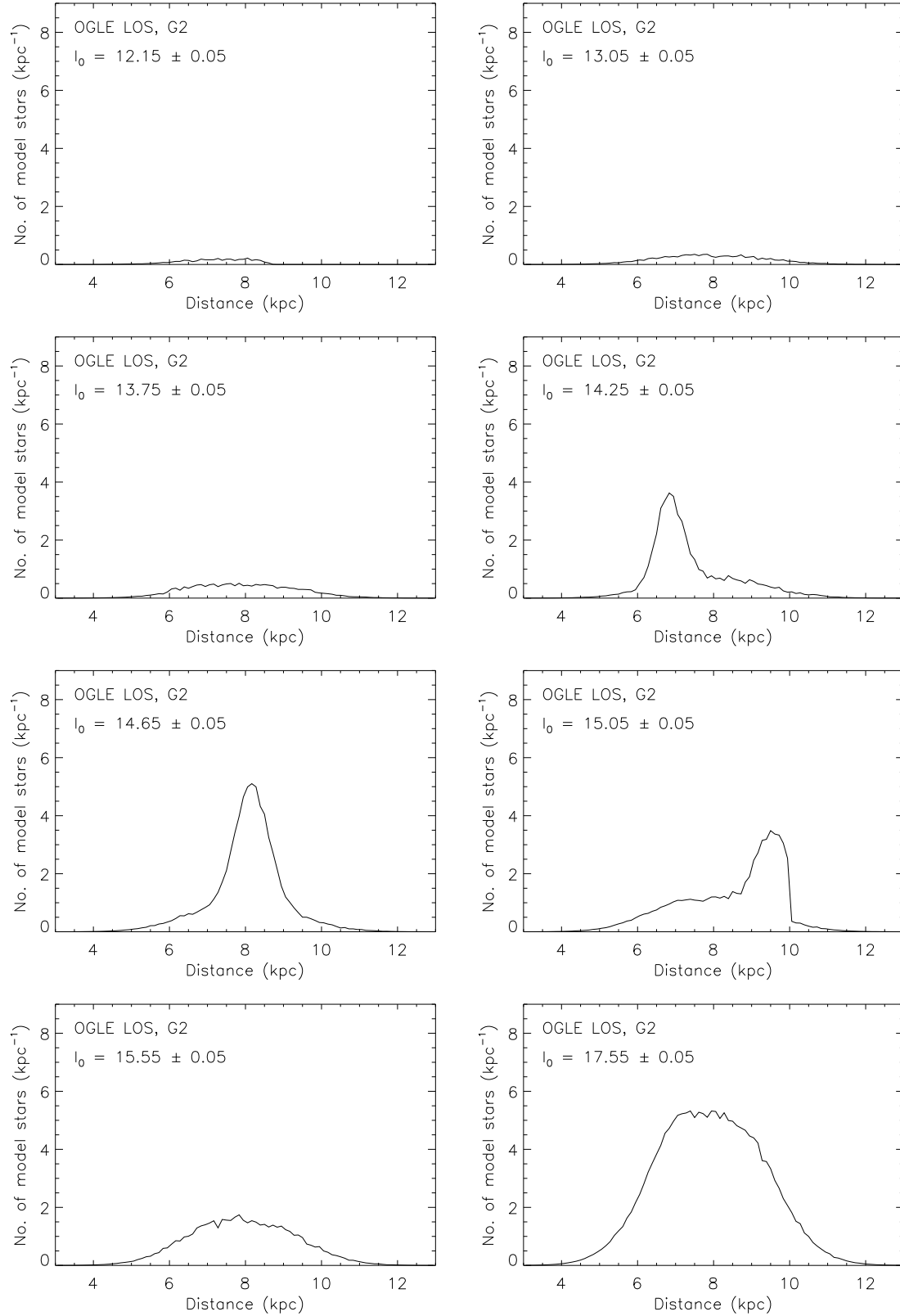


Figure 5. Model source counts as a function of distance (OGLE LOS, G2 model), for selected apparent magnitudes I_0 (with I_0 bin widths of 0.1 mag). These magnitudes are indicated in the panels, and correspond to the slices indicated in Fig. 3 (top panel).

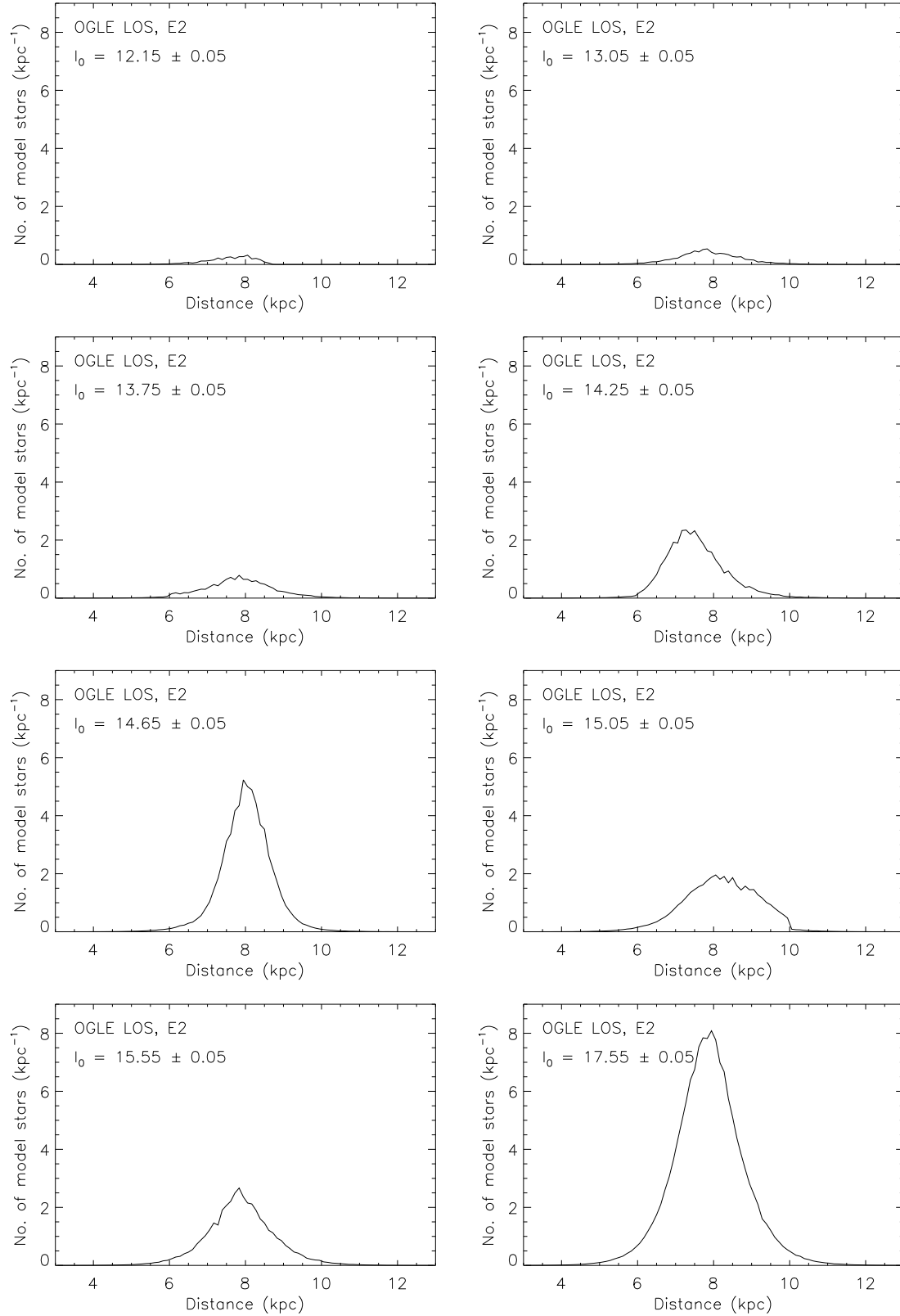


Figure 6. Model source counts as a function of distance. Same as Fig. 5, but for the E2 model, with the selected magnitudes corresponding to the slices indicated in Fig. 4 (top panel).

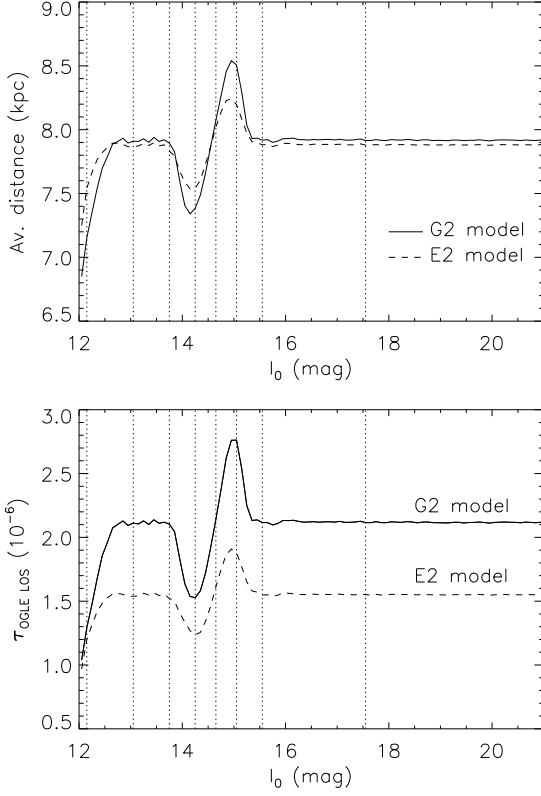


Figure 7. Top panel: average distance of model OGLE LOS sources as a function of magnitude. Bottom panel: $\tau_{\text{OGLE LOS}}$ as a function of magnitude (same as top panel of Fig. 2). The vertical dotted lines correspond to the slice magnitudes indicated in Figs. 3–6.

	$(l, b) (^{\circ})$	$\theta_{\text{bar}, \text{G2}} (^{\circ})$	$\theta_{\text{bar}, \text{E2}} (^{\circ})$
OGLE	(1.16, -2.75)	14.8	19.1
MACHO	(1.50, -2.68)	24.6	31.0

Table 4. 1σ upper limits on θ_{bar} , from combining the expected optical depths with those measured by OGLE and MACHO (see text). Values are shown for the G2 and E2 bar models.

If the given bar angles of the G2 and E2 models are now varied, model-independent trends with θ_{bar} may be revealed. Fig. 8 shows that the expected amplitudes of $\tau_{\text{OGLE LOS}}$, $\tau_{\text{MACHO LOS}}$ and $\tau_{\text{MOA LOS}}$ all decrease with increasing bar angle. This provides a potential constraint on θ_{bar} , should the expected τ amplitude be observed and its magnitude accurately measured. Another constraint is shown by Fig. 9, where the expected optical depths τ_{OGLE} , τ_{MACHO} and τ_{MOA} display a similar dependence on θ_{bar} . The corresponding observed values are overplotted, with their 1σ uncertainties, and from the intersections with the predicted OGLE and MACHO curves, 1σ upper limits on θ_{bar} are obtained. (There is no intersection between the predicted and observed τ_{MOA}). These

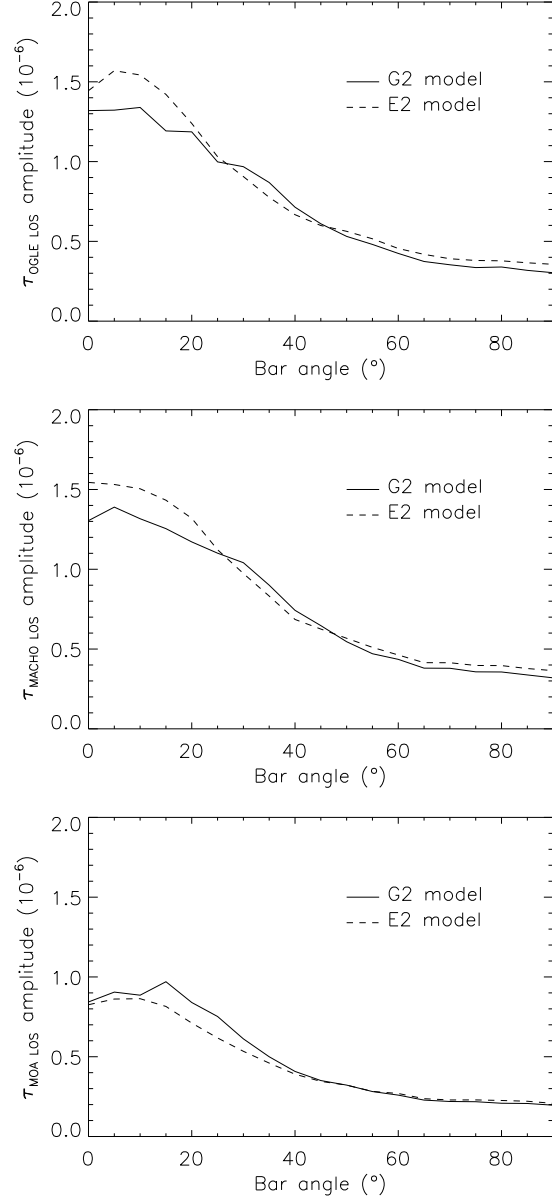


Figure 8. (Top, middle, bottom) panel: oscillation amplitude of expected ($\tau_{\text{OGLE LOS}}$, $\tau_{\text{MACHO LOS}}$, $\tau_{\text{MOA LOS}}$) as a function of θ_{bar} , for the G2 and E2 models.

limits are given in Table 4. Note that they exclude the large bar angle of the E2 model ($\theta_{\text{bar}} = 41.3^{\circ}$), as well as those from GLIMPSE ($\theta_{\text{bar}} = (44 \pm 10)^{\circ}$) and EROS ($\theta_{\text{bar}} = (49 \pm 8)^{\circ}$).

3.2 Comparison with EROS data

The EROS-2 survey (Hamadache et al. 2006) has found the largest sample of clump–giant events so far, 120, compared with 32 and 62 for the latest OGLE and MACHO surveys, respectively. This sample may be sufficient to enable a useful comparison of the predicted optical depth trends with obser-

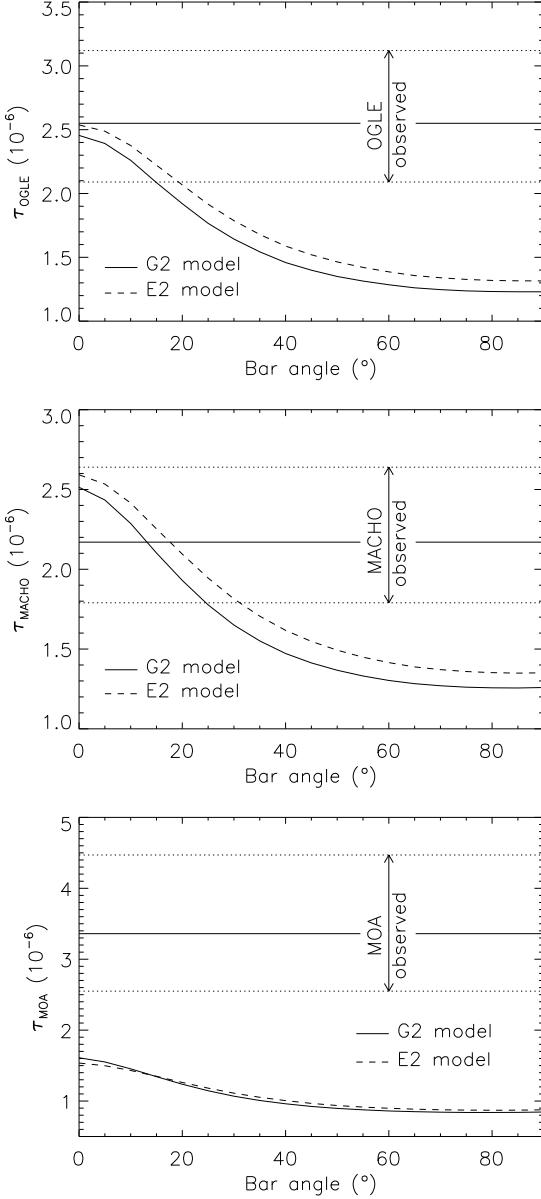


Figure 9. (Top, middle, bottom) panel: expected (τ_{OGLE} , τ_{MACHO} , τ_{MOA}) as a function of θ_{bar} , for the G2 and E2 models. The horizontal lines show the value measured by (OGLE, MACHO, MOA) with its 1σ uncertainties.

vational data. Since the EROS-2 survey (like all microlensing surveys) was conducted across many fields rather than for a specific LOS, any observed oscillation in τ similar to the prediction would be somewhat smoothed out. However, this effect should not be strong, as the predicted trend is similar for different lines of sight towards the bulge (as shown in Fig. 2), and in any case such effects are accounted for as described below.

To make the comparison, unpublished EROS-2 data have been supplied by J. Rich et al. (private communication). They

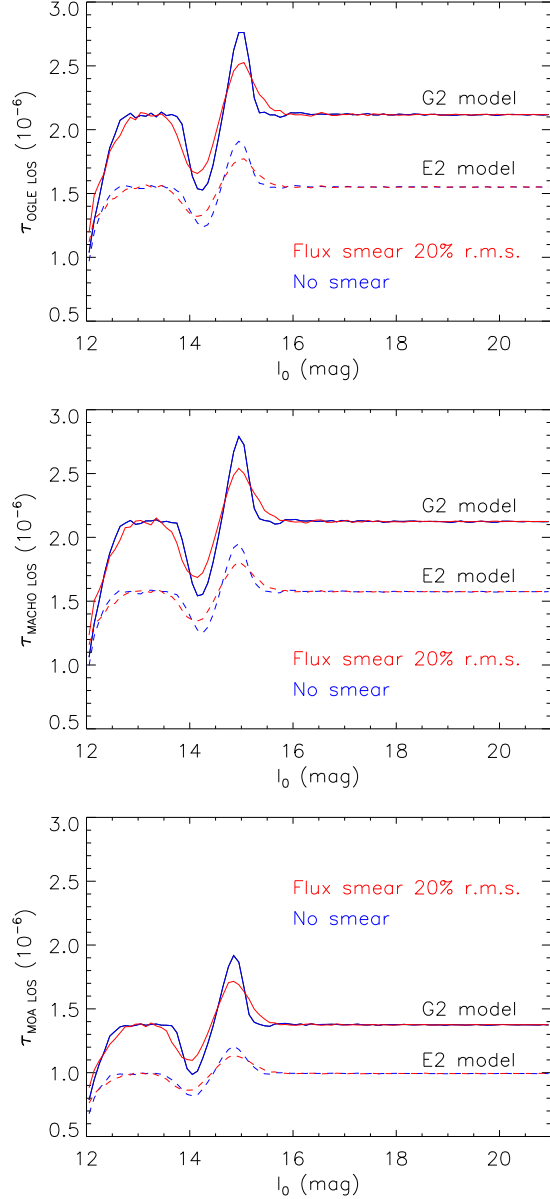


Figure 10. (Top, middle, bottom) panel: expected ($\tau_{\text{OGLE LOS}}$, $\tau_{\text{MACHO LOS}}$, $\tau_{\text{MOA LOS}}$) as a function of source apparent magnitude, with and without stellar flux smearing of 20 per cent rms, as indicated. The curves with no smearing are the same as in Fig. 2.

find, from studies with artificial stars, that clump giant fluxes are smeared by ~ 20 per cent rms, which does not affect their optical depth calculations averaged over the whole clump, but will of course reduce the τ amplitude by smoothing out the predicted oscillation. This flux smearing effect is added to all of the model stars, using a Gaussian with $\sigma = 0.2$. It is found that although the τ amplitude is indeed reduced, the oscillation is still clear, as shown in Fig. 10.

EROS stars were observed in two non-standard bands, R_{EROS} and B_{EROS} , where $R_{\text{EROS}} = I_{\text{OGLE}}$. Hence only the

R_{EROS} data are considered, to avoid any complications arising from using different magnitude scales. Hamadache et al. (2006) divided each of their 66 bulge fields into 32 subfields. For each subfield, they modelled the stellar density in colour–magnitude space as a power-law plus Gaussian, in order to find the magnitude, $R_{\text{EROS, clump}}$, and colour of the clump centre. Hence smoothing effects (as mentioned above) and extinction can now both be easily accounted for here, by taking the clump centres as reference points: instead of simply finding τ as a function of R_{EROS} , it is found as a function of magnitude *relative to the clump centres*, $R_{\text{EROS}} - R_{\text{EROS, clump}}$. This method ‘lines up’ all the clump centres in each subfield. For comparison, the predicted τ is similarly found as a function of $I_0 - I_{0, \text{clump}}$. For the (OGLE, MACHO, MOA) LOS, the Gaussian component shown in Fig. 1 peaks at $I_{0, \text{clump}} = (14.75, 14.65, 14.55) \pm 0.05$ (for bin widths of 0.1 mag). For the E2 model, the magnitudes are slightly brighter: $I_{0, \text{clump}} = (14.65, 14.55, 14.45) \pm 0.05$.

τ_{EROS} is now found as a function of source magnitude using equation (13) from Hamadache et al. (2006):

$$\tau = \frac{\pi}{2u_0(\text{max})} \frac{\sum_{i=1}^{N_{\text{ev}}} t_{\text{E},i} / \epsilon(t_{\text{E},i})}{\sum_{j=1}^{N_*} T_j}, \quad (3)$$

where each event i has a time-scale $t_{\text{E},i}$ and detection efficiency $\epsilon(t_{\text{E},i})$, each monitored star j is observed for a time T_j , the total numbers of events and stars are N_{ev} and N_* , respectively, and the maximum impact parameter $u_0(\text{max}) = 0.75$. This calculation is implemented with a separate summation for each magnitude bin (and taking full account of the different detection efficiencies for each EROS-2 field). The uncertainty is also determined following Hamadache et al. (2006), who added in quadrature a 5 per cent systematic part – due to blending effects – and a larger statistical part, estimated according to Han & Gould (1995).

Fig. 11 shows τ_{EROS} as a function of $R_{\text{EROS}} - R_{\text{EROS, clump}}$. The observed trend is now compared with the flux-smearred predicted trends, using a χ^2 test, to see if the former is better fitted by an oscillating or constant optical depth. Since it is fitting an oscillating *form* that is of interest, the width of the oscillation and the absolute values of the τ amplitude and τ_{flat} are allowed to vary as free parameters in the fit: the model trend may be stretched along the magnitude axis, and both shifted and stretched along the τ axis – though not

stretched in the former case by more than an arbitrary limit of 50 per cent, since Fig. 2 shows that the width of the oscillation does not vary much with direction. Finally, to allow for other slight changes in the shape of the oscillation with direction and bulge model, all six of the predicted trends (three lines of sight, G2 and E2 models) are tested. These χ^2 values are compared with that for a freely-fitted constant optical depth. The results are shown in Table 5. Also indicated are the chance probabilities p that χ^2 would be greater than or equal to the given values.

An oscillating τ appears to provide a better fit to the data than a constant optical depth. There is a mostly negligible change in χ^2 with direction, and a small but insignificant preference for the E2 model. Fig. 11 shows the best-fit oscillation, with the MACHO E2 trend: τ_{flat} has been shifted by -0.05×10^{-6} , and the curve has been stretched by factors of 1.50 and 1.60 along the magnitude and τ axes, respectively. (Note that the factor of 1.50 is at the (arbitrary) 50 per cent limit. The fits improve with further magnitude stretching, the best possible fit being for a factor of 2.50 (MACHO G2 model), with $\chi^2 = 1.44$, but this is well beyond the limit and is ignored). However, the significance of the χ^2 preference for an oscillating τ , rather than a constant value, is low. A reasonable magnitude binning gives only eight data points. Whereas the oscillating τ fit has three free parameters and five degrees of freedom, the constant τ fit has of course just one free parameter, and seven degrees of freedom. The constant τ fit is not significantly discrepant to the data.

It is possible that the EROS-2 event detection efficiency may be a function of magnitude. However, it would not be a strong dependance, and any variation would be smooth. It could not therefore hide any real oscillation of τ , or generate a false one (J. Rich, private communication). It appears that the available data are still insufficient to accurately determine the dependance of the optical depth on source apparent magnitude.

However, there is another, simpler way to look for signs of the predicted τ oscillation in the survey data. If τ is indeed higher on the faint side of the clump centres, then more of the observed events should also be on the faint side: a plot of event counts, as a function of $R_{\text{EROS}} - R_{\text{EROS, clump}}$, should be noticeably skewed towards the faint side. Fig. 12 shows that this

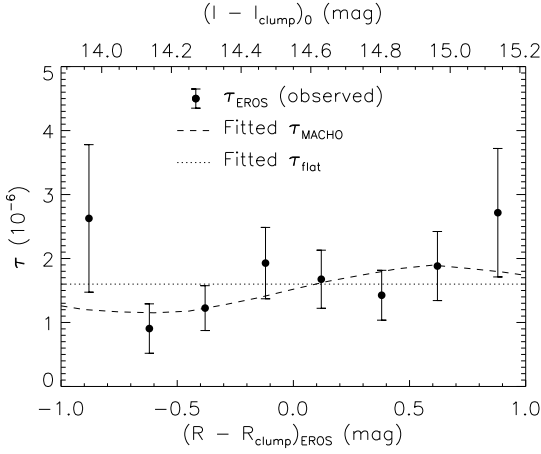


Figure 11. Observed τ_{EROS} , and fitted model τ_{MACHO} LOS, as functions of magnitude relative to the clump centre, $R_{EROS} - R_{EROS, clump}$ and $I_0 - I_{0, clump}$, respectively (see text). The latter magnitude scale is stretched relative to the former by the fitting factor. Also shown is the fitted τ_{flat} .

	G2	E2
OGLE	2.07	1.84
MACHO	1.91	1.83
MOA	1.99	1.93
Average	1.99	1.87
	($p > 0.75$)	($p > 0.75$)
Constant τ	4.24	
	($p > 0.75$)	
$\Delta\chi^2$	2.25	2.37

Table 5. χ^2 values from fitting the observed τ_{EROS} as a function of $R_{EROS} - R_{clump}$ with the predicted (oscillating) trends, for different lines of sight and bulge models as indicated, and with a constant optical depth. Also indicated are the chance probabilities p that χ^2 would be greater than or equal to the given values. An oscillating τ provides a better fit, but at a low significance (see text).

is so. The ratio of events with $R_{EROS} - R_{EROS, clump}$ fainter than zero to those brighter than zero (hereafter the *skewness ratio*) is 1.14. The significance of this skew is tested as follows. The plot of event counts is fitted with a Gaussian, as shown. This is of course an imperfect fit, but gives an approximate measure of the dispersion. Then 120 points (for the 120 EROS events) are randomly distributed on the magnitude axis, according to a Gaussian with the fitted dispersion, and the skewness ratio is calculated. For one million such Monte Carlo cases, only 21 per cent have a skewness ratio greater than the observed value. Thus the observed skew is suggestive, but not highly significant.

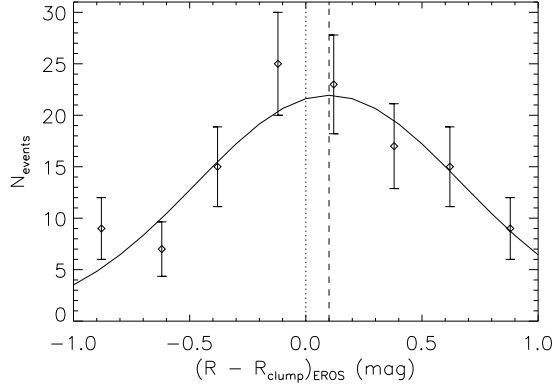


Figure 12. EROS event counts as a function of magnitude relative to the clump centre, $R_{EROS} - R_{EROS, clump}$. The error bars represent Poisson uncertainties. The distribution is skewed towards the faint side of the magnitude axis; the trend is fitted with a Gaussian in order to test the significance of the skew (see text). The vertical dotted line indicates $R_{EROS} - R_{EROS, clump} = 0$, and the vertical dashed line indicates the centre of the Gaussian.

4 SUMMARY AND CONCLUSIONS

It does not appear that the discrepancy in optical depth measurements between the RCG and all-star analyses can be explained by a dependence of the lensing surveys on their flux limits. The model reproduces the OGLE and MACHO values based on RCGs, but underpredicts MOA's all-star value by $\sim 2.4\sigma$. Another potential explanation for the discrepancy is blending. Sumi et al. (2006) found ~ 38 per cent of OGLE-II events with apparent RCG sources were really due to faint stars blended with a bright companion. However, they also showed that blending has little effect on estimates of τ due to partial cancellation of its different effects, a point also made by Popowski et al. (2005) and Hamadache et al. (2006). Sumi et al. (2006) also state that the DIA method is less sensitive to the systematics of blending in crowded fields. Though it is of course possible that MOA's value may yet be lowered with more data, it is supported by MACHO's earlier DIA value.

τ is expected to be generally constant as a function of source apparent magnitude for $I_0 \gtrsim 13.0$, except in the range $13.5 \lesssim I_0 \lesssim 15.5$, where many RCGs are detected. These stars dominate the source counts at such magnitudes, and show a strong correlation between distance and apparent magnitude, causing a significant oscillation in τ . The amplitude of this oscillation is found to decrease with increasing bar angle, providing a potential constraint on θ_{bar} . A further constraint

comes from a similar dependance of τ with θ_{bar} : combining the predicted trends with the measured values provides 1σ upper limits, which exclude the large bar angles reported by GLIMPSE and EROS.

From the EROS-2 survey, τ_{EROS} has been found as a function of source apparent magnitude. The predicted oscillation is not only consistent with the observed trend, but provides a better χ^2 fit than a constant optical depth, though the significance of this preference is low due to insufficient data. However, a further sign comes from EROS event counts, which show a clear skew towards fainter magnitudes. With ongoing surveys detecting increasing numbers of RCG events (and $\sim 500 \text{ yr}^{-1}$ of all kinds), it should soon be possible to make a more useful and definite comparison.

ACKNOWLEDGMENTS

I am grateful to Jim Rich of the EROS collaboration for providing their data, and for his helpful comments. I also thank Szymon Kozłowski, Shude Mao and Łukasz Wyrzykowski for useful discussions, and the anonymous referee for their comments. I acknowledge support from a PPARC studentship, and travel support from the European Community's Sixth Framework Marie Curie Research Training Network Programme, Contract No. MRTN-CT-2004-505183 'ANGLES'.

REFERENCES

- Afonso C. et al., 2003, *A&A*, 404, 145
 Alcock C. et al., 2000, *ApJ*, 541, 734
 Benjamin R.A. et al., 2005, *ApJ*, 630, L149
 Dwek E. et al., 1995, *ApJ*, 445, 716
 Gerhard O., 2002, in Da Costa G.S., Sadler E.M., eds., *ASP Conf. Ser. Vol. 273, The Dynamics, Structure & History of Galaxies: A Workshop in Honour of Professor Ken Freeman*, Astron. Soc. Pac., San Francisco, p. 73
 Hamadache C. et al., 2006, *A&A*, 454, 185
 Han C., Gould A., 1995, *ApJ*, 449, 521
 Han C., Gould A., 2003, *ApJ*, 592, 172
 Popowski P. et al., 2005, *ApJ*, 631, 879
 Stanek K.Z., 1995, *ApJ*, 441, L29
 Stanek K.Z., Mateo M., Udalski A., Szymański M., Kaluźny J., Kubiak M., 1994, *ApJ*, 429, L73
 Sumi T., 2004, *MNRAS*, 349, 193
 Sumi T. et al., 2003, *ApJ*, 591, 204
 Sumi T. et al., 2006, *ApJ*, 636, 240
 Thomas C.L. et al., 2005, *ApJ*, 631, 906
 Udalski A. et al., 2002, *Acta Astron.*, 52, 217
 Wood A., Mao S., 2005, *MNRAS*, 362, 945
 Woźniak P.R., Udalski A., Szymański M., Kubiak M., Pietrzyński G., Soszyński I., Żebruń K., 2001, *Acta Astron.*, 51, 175
 Zheng Z., Flynn C., Gould A., Bahcall J.N., Salim S., 2001, *ApJ*, 555, 393